Supporting Information

Article title: A process-based representation of hydraulic activation of stomata induced by hygroscopic fertilizer salts in the ORCHIDEE-CROP model (v2.2)

Authors: Shuaishuai Deng [1], Jürgen Burkhardt [2], Ronny Lauerwald [1], Christophe Flechard [3], Jürgen Knauer [4], Benjamin Dumont [5], Emilio Baud-Fraile [1], Yang Su [1], Ke Yu [6], Nicolas Viovy [7], Benjamin Loubet [1]

Affiliations

[1] UMR ECOSYS, INRAE AgroParisTech, Université Paris-Saclay, 91120 Palaiseau, France

[2] Institute of Crop Science and Resource Conservation, University of Bonn, Bonn, Germany

[3] UMR 1069 SAS, INRAE, Institut Agro, Rennes, 35042, France

[4] School of Life Sciences, Faculty of Science, University of Technology Sydney, Ultimo, NSW 2007, Australia

[5] ULiege-Gembloux AgroBio-Tech, Plant Sciences Axis, Crop Science Lab., B-5030 Gembloux, Belgium

[6] International Institute for Applied Systems Analysis (IIASA), Schlossplatz 1, 2361 Laxenburg, Austria

[7] Laboratoire des Sciences du Climat et de l'Environnement, IPSL, CEA-CNRS-UVSQ, Université Paris-Saclay, Gif-sur-Yvette, France

The following Supporting Information is available for this article:

Figure S1. Calibration of N_{ref} from event-scale transpiration anomalies at FR-Gri.

Figure S2. Surface energy and microclimatic responses to HAS at FR-Gri and BE-Lon.

Figure S3. Sensitivity of event-scale LE evaluation to event-window length at FR-Gri and BE-Lon.

Figure S4. Sensitivity of event-scale LE performance to HAS parameters at FR-Gri and BE-Lon.

Figure S5. Environmental and process diagnostics of simulated HAS responses at FR-Gri and BE-Lon.

Figure S6. Water deficit sensitivity of the simulated HAS effect on latent heat flux.

Table S1. Site characteristics and simulation periods of the four cropland sites used in this study.

Table S2. Fertilization management at FR-Gri.

Table S3. Fertilization management at FR-EM2.

Table S4. Fertilization management at BE-Lon.

Table S5. Fertilization management at US-Ne1.

Table S6. Original evaporative efficiency terms in ORCHIDEE-CROP and HAS implementation in this study.

Table S7. Four-site summary of the reference HAS simulation during 0–10 d post-UAN event windows.

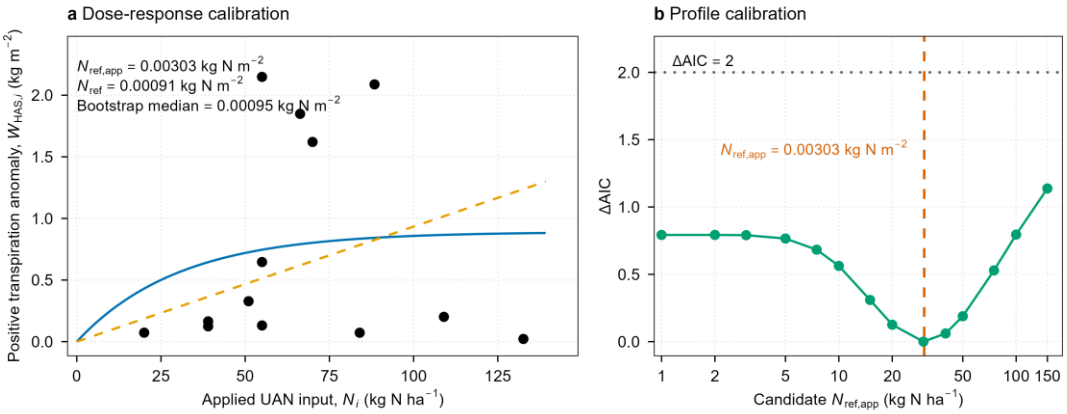


Figure S1. Calibration of the reference UAN amount (N_{ref}) from event-scale transpiration anomalies at FR-Gri. (a) Relationship between the event-scale positive transpiration anomaly, $W_{HAS,i}$, and applied UAN input, N_i. The blue curve shows the fitted saturating dose–response relationship used to estimate the reference applied UAN amount, $N_{ref,app}$, and the orange dashed line shows the no-intercept linear fit for comparison. The fitted $N_{ref,app}$ was 0.00303 kg N m^{-2}, corresponding to a retained reference amount of N_{ref} = 0.00091 kg N m^{-2} using the prescribed throughfall fraction f_{tf} = 0.7. (b) Profile calibration of $N_{ref,app}$ based on ΔAIC. The vertical dashed line indicates the fitted $N_{ref,app}$, and the horizontal dotted line indicates ΔAIC = 2. The broad range of candidate values below this threshold indicates relatively weak constraint on $N_{ref,app}$.

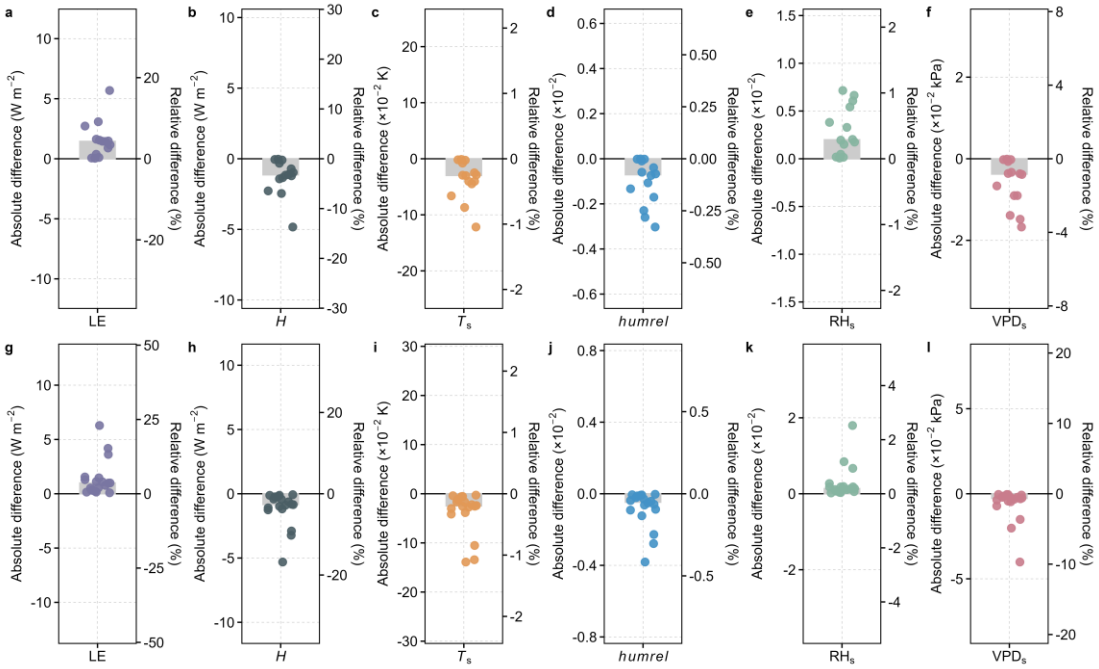


Figure S2. Surface energy and microclimatic responses to HAS at FR-Gri (a–f) and BE-Lon (g–l). Event-level differences between ORC-HAS and ORC-STD during the 0–10 d post-UAN period are shown for (a, g) latent heat flux (LE), (b, h) sensible heat flux (*H*), (c, i) surface temperature (T_s), (d, j) soil moisture stress factor (*humrel*), (e, k) surface relative humidity (RH_s), and (f, l) surface vapor pressure deficit (VPD_s). Left axes show absolute differences, calculated as ORC-HAS minus ORC-STD. Right axes show the corresponding relative differences, calculated as (ORC-HAS − ORC-STD) / ORC-STD × 100. Points represent individual UAN events, and gray bars indicate median event-level differences.

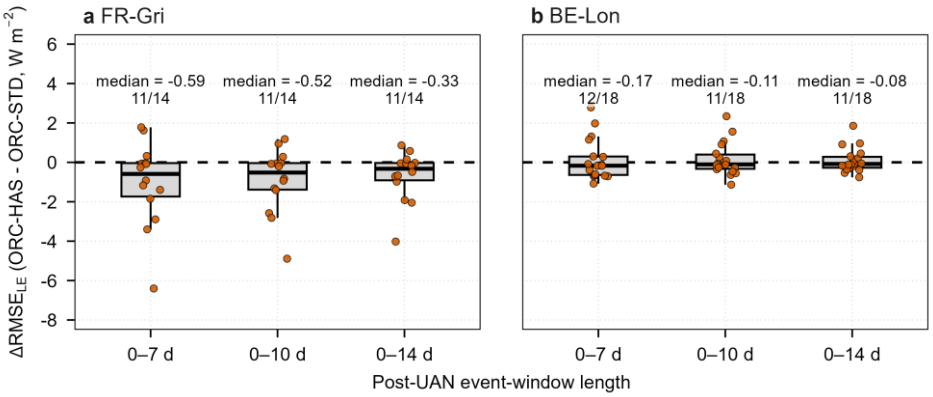


Figure S3. Sensitivity of event-scale latent heat flux (LE) evaluation to event-window length at FR-Gri (a) and BE-Lon (b). Event-scale changes in $RMSE_{LE}$ were calculated as $\Delta RMSE_{LE}$ = RMSE_ORC-HAS − RMSE_ORC-STD for 0–7 d, 0–10 d, and 0–14 d post-UAN evaluation windows. Points indicate individual UAN events, and boxplots summarize the event distributions. Negative $\Delta RMSE_{LE}$ values indicate improved LE performance under ORC-HAS relative to ORC-STD. Text labels show the median $\Delta RMSE_{LE}$ and the number of events with improved $RMSE_{LE}$ relative to the total number of events.

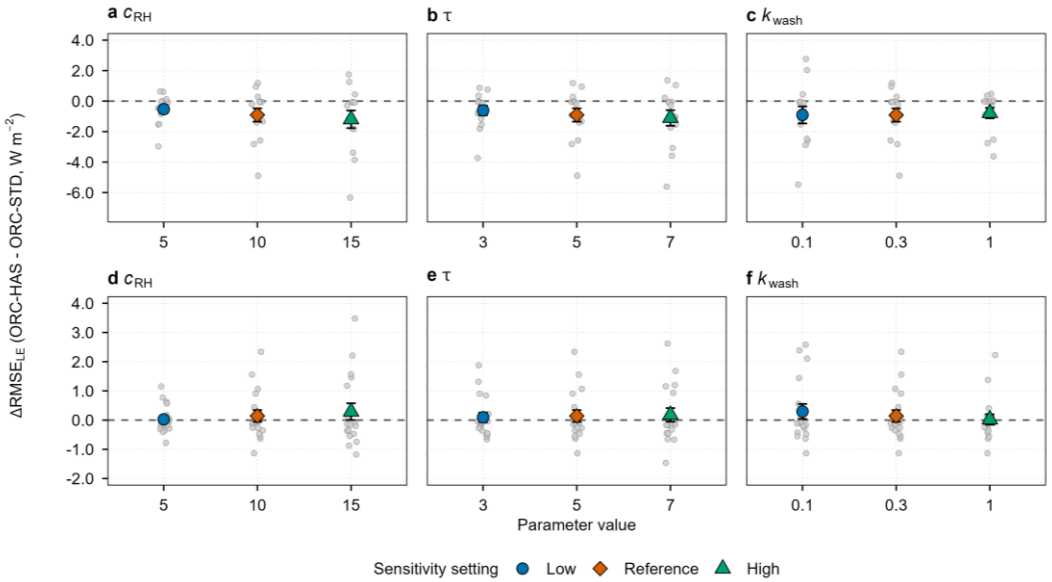


Figure S4. Sensitivity of event-scale latent heat flux (LE) performance to HAS parameters at FR-Gri (a–c) and BE-Lon (d–f). Panels show responses to the RH-scaling coefficient c_{RH} (a, d), the dry depletion timescale τ (b, e), and the wash-off coefficient k_{wash} (c, f). Event-scale changes in $RMSE_{LE}$ were calculated as $\Delta RMSE_{LE}$ = RMSE_ORC-HAS – RMSE_ORC-STD during the 0–10 d post-UAN event windows. Negative values indicate improved LE performance under ORC-HAS. Gray points indicate individual UAN events, and colored symbols with error bars indicate means ± SE. Blue, orange, and green symbols represent the low, reference, and high parameter settings, respectively.

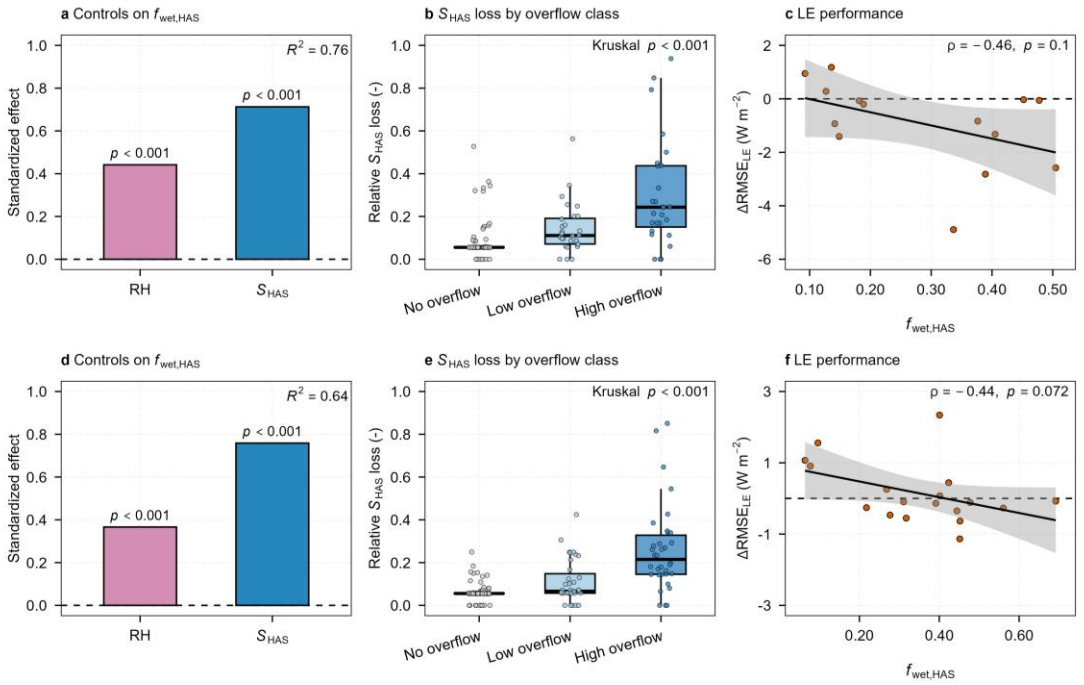


Figure S5. Environmental and process diagnostics of simulated HAS responses at FR-Gri (a–c) and BE-Lon (d–f). (a, d) Relative controls of RH and S_{HAS} on $f_{wet,HAS}$ during non-overflow days. Standardized effects were estimated from rank-based regressions of $f_{wet,HAS}$ against RH and S_{HAS}; larger positive values indicate stronger positive associations with $f_{wet,HAS}$. (b, e) S_{HAS} loss after accounting for dry depletion across overflow classes. Overflow days were divided into low- and high-overflow classes using the median of non-zero $q_{overflow}$ values, while days with $q_{overflow} \leq 1 \times 10^{-12}$ were classified as non-overflow days. (c, f) Relationship between event-mean $f_{wet,HAS}$ and $\Delta RMSE_{LE}$ across UAN events. Negative $\Delta RMSE_{LE}$ values indicate improved LE performance under ORC-HAS relative to ORC-STD. Event windows covered 0–10 d after UAN application.

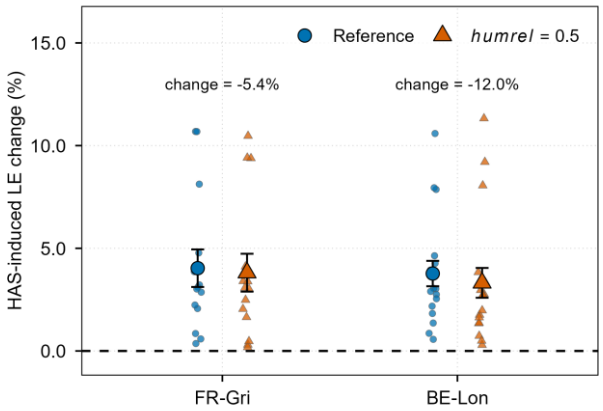


Figure S6. Water deficit sensitivity of the simulated HAS effect on latent heat flux. The net relative effect of HAS on latent heat flux (LE) was calculated as (ORC-HAS − ORC-STD) / ORC-STD × 100 during the 0–10 d post-UAN event windows. Reference simulations are compared with prescribed water deficit simulations in which *humrel* was set to 0.5 in both ORC-HAS and ORC-STD. Points indicate individual UAN events, and large symbols with error bars indicate means ± SE. Text labels show the relative change in the mean net HAS effect on LE under *humrel* = 0.5 compared with the reference simulation.

Table S1. Site characteristics and simulation periods of the four cropland sites used in this study.

Site	Years	Latitude	Longitude	Studied crop species	Soil texture
FR-Gri	2005–2020	48.84° N	1.95° E	Winter wheat	Clay loam
FR-EM2	2017–2021	49.87° N	3.02° E	Winter wheat	Clay loam
BE-Lon	2005–2020	50.55° N	4.74° E	Winter wheat	Clay loam
US-Ne1	2013–2022	41.16° N	96.47° W	Maize	Silty clay loam

Table S2. Fertilization management at FR-Gri. The applied liquid nitrogen fertilizer consisted of 25% NO_3^-, 25% NH_4^+, and 50% $CO(NH_2)_2$. The table lists crop species, sowing to harvest dates, UAN application dates, and application rates (kg N ha^{-1}).

Crop species	Sowing–harvest date	UAN application date	Rate (kg N ha^{-1})
Winter wheat	10/28/2005–7/15/2006	3/15/2006	55.0
		4/14/2006	55.0
Winter wheat	10/17/2008–7/31/2009	3/2/2009	58.0
		3/30/2009	109.0
Winter wheat	10/20/2011–8/3/2012	5/7/2012	70.0
Winter wheat	10/8/2013–8/5/2014	3/14/2014	51.0
		3/28/2014	39.0
		5/16/2014	20.0
Winter wheat	10/20/2015–7/28/2016	3/1/2016	84.0
		4/9/2016	39.0
		5/10/2016	55.0
Winter wheat	9/25/2017–7/8/2018	3/16/2018	38.0
		5/12/2018	39.0
Winter wheat	10/2/2019–7/10/2020	3/4/2020	300 (L ha^{-1})
		4/6/2020	150 (L ha^{-1})
		4/29/2020	200 (L ha^{-1})

Table S3. Fertilization management at FR-EM2. The applied liquid nitrogen fertilizer consisted of 25% NO_3^-, 25% NH_4^+, and 50% $CO(NH_2)_2$. The table lists crop species, sowing to harvest dates, UAN application dates, and application rates (kg N ha^{-1}). The 2015 record was excluded from model evaluation because flux data were unavailable.

Crop species	Sowing–harvest date	UAN application date	Rate (kg N ha^{-1})
Winter wheat	10/31/2014–7/31/2015	4/11/2015	60.0
Winter wheat	10/16/2017–7/13/2018	4/12/2018	40.0
		5/2/2018	40.0
Winter wheat	10/26/2020–8/14/2021	4/9/2021	69.81

Table S4. Fertilization management at BE-Lon. The applied liquid nitrogen fertilizer consisted of 25% NO_3^-, 25% NH_4^+, and 50% $CO(NH_2)_2$. The table lists crop species, sowing to harvest dates, UAN application dates, and application rates (kg N ha^{-1}).

Crop species	Sowing–harvest date	UAN application date	Rate (kg N ha^{-1})
Winter wheat	10/14/2004–8/3/2005	3/22/2005	45.0
		4/12/2005	35.0
Winter wheat	10/13/2006–8/5/2007	3/17/2007	40.0
		4/12/2007	60.0
Winter wheat	11/13/2008–8/7/2009	3/18/2009	80.0
		4/24/2009	40.0
Winter wheat	10/13/2010–8/16/2011	3/12/2011	58.5
		4/6/2011	39.0
Winter wheat	10/25/2012–8/12/2013	4/16/2013	97.5
		5/7/2013	23.4
		5/21/2013	70.2
Winter wheat	10/14/2014–8/2/2015	3/14/2015	58.5
		4/15/2015	39.0
		5/11/2015	78.0
Winter wheat	10/29/2016–7/29/2017	3/16/2017	68.3
		4/12/2017	39.0
Winter wheat	10/10/2018–8/1/2019	3/25/2019	58.5
		4/17/2019	39.0

Table S5. Fertilization management at US-Ne1. The applied liquid nitrogen fertilizer consisted of 25% NO_3^-, 25% NH_4^+, and 50% $CO(NH_2)_2$. The table lists crop species, UAN application dates, and application rates (kg N ha^{-1}).

Crop species	UAN application date	Rate (kg N ha^{-1})
Maize	4/22/2014	123.3
	7/3/2014	39.2
Maize	5/12/2015	33.6
	5/18/2015	33.6
	7/4/2015	38.1
Maize	7/2/2017	54.9
Maize	4/21/2020	45.1
	6/24/2020	44.8
Maize	7/6/2021	22.1

Table S6. Original evaporative efficiency terms and HAS implementation in ORCHIDEE-CROP. The table summarizes the original β-based latent heat flux partitioning terms used in ORCHIDEE-CROP and the additional HAS-related term implemented in this study. The notation follows the manuscript: f_{crop} is the current crop fraction, f_{int} is the intercepted-water fraction of the canopy, f_{res} is the canopy exchange limitation factor, and $f_{wet,HAS}$ is the relative humidity-dependent effective HAS wet fraction.

Term	Process represented	Implementation	Role in the HAS implementation
β_1	Snow sublimation	Calculated in diffuco_snow as vbeta1 from snow-covered surface fractions and available snow storage.	Original ORCHIDEE-CROP term; unchanged.
β_2	Canopy interception loss	Calculated in diffuco_inter as vbeta2 from the intercepted water fraction. In manuscript notation, this corresponds to evaporation from the rainfall-wetted canopy fraction f_{int}.	Original ORCHIDEE-CROP term; retained separately so that HAS wetting does not double count the rainfall-intercepted canopy area.
β_3	Transpiration	Calculated in diffuco_trans_co2 as vbeta3. In manuscript notation, transpiration is controlled by f_{crop}, $1 - f_{int}$, and f_{res}, with additional treatment of wetted foliage after interception water is depleted.	Original ORCHIDEE-CROP term; provides the canopy exchange limitation factor f_{res} used to scale β_{HAS}.
β_4	Bare soil evaporation	Calculated in diffuco_bare as vbeta4 from the bare-soil evaporation limitation and remaining evaporative fraction.	Original ORCHIDEE-CROP term; unchanged.
β_{HAS}	HAS evaporative efficiency	Calculated in diffuco_has as vbeta_has. $\beta_{HAS} = f_{crop} f_{wet,HAS} f_{res}$.	New term representing the additional liquid water loss pathway associated with hygroscopic salt films.
Total β	Total evaporative efficiency	Original formulation: $\beta = \beta_2 + \beta_3 + \beta_4$. With HAS: $\beta = \beta_2 + \beta_3 + \beta_4 + \beta_{HAS}$.	Defines how the new HAS pathway is incorporated into the existing LE partitioning framework.

Table S7. Four-site summary of the reference HAS simulation during 0–10 d post-UAN event windows. The net effect of HAS on LE was calculated as LE_ORC-HAS − LE_ORC-STD, and the relative net effect (%) was calculated as (LE_ORC-HAS − LE_ORC-STD) / LE_ORC-STD × 100. The feedback offset (%) represents the fraction of direct HAS water loss offset by soil water feedback and is reported as the mean across events with non-zero direct HAS water loss at each site. Net HAS effects on LE are reported as event means averaged by site, whereas $\Delta RMSE_{LE}$, ΔMAE_{LE}, and $\Delta|Bias|_{LE}$ are reported as site-level medians of event-scale paired differences between ORC-HAS and ORC-STD. Mean IWUE change (%) was calculated as the event-level relative difference between ORC-HAS and ORC-STD and then averaged by site. Negative $\Delta RMSE_{LE}$, ΔMAE_{LE}, and $\Delta|Bias|_{LE}$ indicate improved performance under ORC-HAS relative to ORC-STD. S_{HAS}, $f_{wet,HAS}$, and β_{HAS} are dimensionless.

Site	Crop	Years	N events total	Net HAS effect on LE (W m^{-2})	Net HAS effect on LE (%)	Mean feedback offset (%)	Median $\Delta RMSE_{LE}$ (W m^{-2})	RMSE improved events	RMSE improved (%)	Median ΔMAE_{LE} (W m^{-2})	Median $\Delta|Bias|_{LE}$ (W m^{-2})	Mean IWUE change (%)	Mean S_{HAS}	Mean $f_{wet,HAS}$	Mean β_{HAS}
FR-Gri	Winter wheat	2005–2020	14	1.55	4.0	14.9	–0.52	11	78.6	–0.58	–1.17	–5.3	0.22	0.28	0.011
BE-Lon	Winter wheat	2005–2020	18	1.41	3.8	13.3	–0.11	11	61.1	–0.06	–0.24	–5.1	0.25	0.35	0.014
FR-EM2	Winter wheat	2017–2021	3	1.79	2.9	17.5	–0.64	3	100.0	–0.91	–0.91	–4.2	0.20	0.33	0.018
US-Ne1	Maize	2013–2022	9	2.15	2.0	24.9	–0.38	6	66.7	–0.77	–0.78	–4.0	0.21	0.29	0.006